Thermo-Mechanical Modelling of Laser Beam Welding of Molybdenum

K.-H. Leitz[1*]
[1]Plansee SE, Metallwerk-Plansee-Straße 71, 6600 Reutte, Austria
*Corresponding author: karl-heinz.leitz@plansee.com

Abstract

Laser beam welding of molybdenum offers enormous potential for a wide variety of high temperature applications. However, due to the high melting temperature and good thermal conductivity of this refractory metal, temperature gradients during the welding process are generally high, causing residual stresses in the weld seam that can lead to an undesired distortion or crack formation. Multi-physical simulations are a powerful tool to get a fundamental understanding of those processes and to develop strategies to minimize distortion and the risk for crack formation. In this contribution a thermo-mechanical modelling approach for laser beam welding is presented. Emanating from a blind seam laser beam welding of molybdenum sheets in overlap configuration is simulated considering contact between the joint partners and clamping. The presented simulation model is applied to analyze the influence of different strategies in laser beam welding of molybdenum sheet material.

Introduction

Laser beam welding is a key technology in industrial manufacturing as it combines high flexibility and the potential for automation with excellent joint quality and minimal thermal influence on the workpiece. Whereas for materials like steel and aluminum laser beam welding is already widely applied in industrial fabrication routes, its application for the joining of high melting metals like molybdenum and tungsten is still in its initial stages. As refractory metals generally exhibit only limited weldability [1, 2], in many high temperature applications, so far riveted joints are still widely applied. There is an enormous potential for the application of laser beam welding in high temperature applications ranging from furnace construction over crystal growth crucible fabrication, shieldings for x-ray technology to nuclear fusion components. Apart from metallurgical issues that must be solved for the fusion welding of refractory metals [3, 4] the high melting temperatures and good thermal conductivities of these metals lead to high temperature gradients during the welding process, causing high residual stresses in the weld seam. Those residual stresses have their origin in plastic deformation due to thermal expansion and contraction of the weld material. They can lead to an undesired distortion of the workpiece or can initiate crack formation. Multi-physical simulations are a powerful tool to get a fundamental process understanding and to develop strategies to avoid those effects. Simulation approaches range from micro-scale thermo-fluid dynamic process simulation [5 - 8] to macro-scale simulation of weld distortion [9 - 10]. [11] gives a good overview about the state of the art in laser beam welding simulation.

Simulation Model

The multi-physical thermo-mechanical simulation model for laser beam welding is set up in Comsol Multiphysics. It utilizes the Heat Transfer, the Structural Mechanics and the Nonlinear Structural Materials Module.

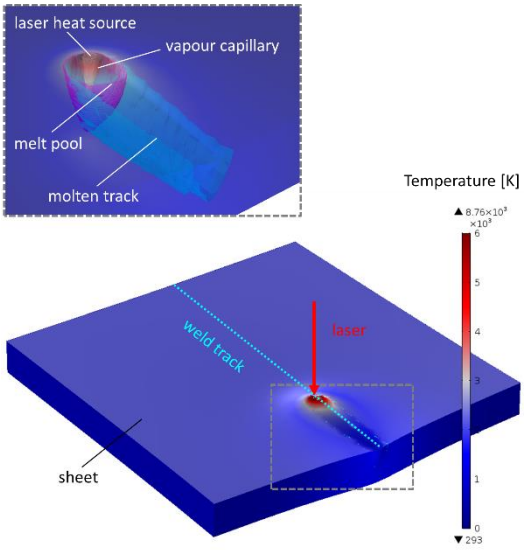

Figure 1. Simulation model for laser beam welding.

Figure 1 shows the simulation configuration for a blind seam with the laser heat source as well as the calculated vapor capillary, melt pool and molten track.

The thermal calculation is based on the heat conduction equation. The energy input by the laser beam is modelled by a moving Gaussian heat source Q_l with exponential decay in the workpiece, approximating the absorption of the laser radiation in the vapor capillary:

$$Q_l = \frac{4A_l P_l}{\pi r_l^2 d_k} \cdot e^{-\frac{2\tilde{r}^2}{r_l^2}} \cdot e^{\frac{2(z-z_0)}{d_k}}.$$

A_l is the assumed absorption degree of the laser radiation, P_l the laser power, r_l the focus radius of the laser beam, d_k the assumed keyhole depth, $\tilde{r}$ the lateral distance to the laser position, z the vertical position and z_0 the position of the sheet surface. The heat transfer calculation considers the latent heats of fusion and evaporation, respectively. For a tracking of the melt pool and the vapor capillary phase functions Φ_m and Φ_v depending on the calculated temperature T of the material are defined:

$$\Phi_m = \begin{cases} 1 & \text{for } T \geq T_m \\ 0 & \text{for } T < T_m \end{cases},$$

$$\Phi_v = \begin{cases} 1 & \text{for } T \geq T_v \\ 0 & \text{for } T < T_v \end{cases}.$$

T_m is the absolute melting temperature and T_v is the absolute evaporation temperature of the sheet material.
The energy loss by evaporation is considered by a heat sink Q_v in the region of the vapor capillary defined by the following term:

$$Q_v = -\frac{H\dot{m}\phi_v}{h}.$$

H is the enthalpy, $\dot{m}$ the evaporation rate, ϕ_v the vapor phase function and h the element size.
The evaporation rate $\dot{m}$ is calculated on the base of the Hertz-Knudsen formula [12]:

$$\dot{m} = (p_v(T) - p_0)\sqrt{\frac{M}{2\pi RT}}.$$

$p_v(T)$ is the vapor pressure at absolute temperature T, p_0 the ambient pressure, M is the molar mass and R the ideal gas constant. The vapor pressure is defined by

$$p_v(T) = p_0 e^{\frac{H_v M}{R}\left(\frac{1}{T_v} - \frac{1}{T}\right)}.$$

with the evaporation enthalpy H_v and the absolute evaporation temperature T_v.
In addition, at the free boundaries convective heat and thermal radiation losses are considered. For the convective heat loss a heat transfer coefficient of 25 W/(m²K) and for the thermal radiation emission an emissivity of 0.2 is assumed. The ambient temperature is defined as 293 K.

In the melt pool (index m) the mechanical material behavior is approximated by a reduction of the elastoplastic material properties Young's modulus E, initial yield stress σ_y and isotropic tangent modulus E_t in the solid (index s) by a scaling factor f:

$$E_m = \frac{E_s}{f},$$

$$\sigma_{ym} = \frac{\sigma_{ys}}{f},$$

$$E_{tm} = \frac{E_{ts}}{f}.$$

In the present work a scaling factor of f = 10 is applied. The reduction of the elastoplastic material properties is sketched in Figure 2. It leads to an almost stress-free melt pool (see Figure 3).

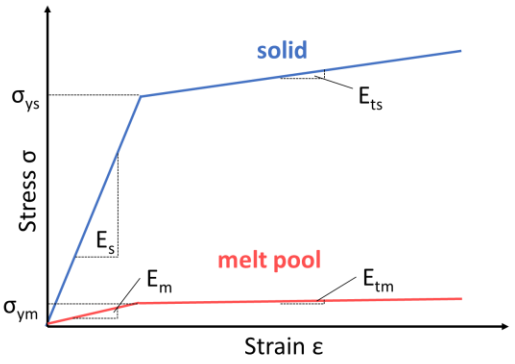

Figure 2. Reduction of elastoplastic material properties in the melt pool.

a)

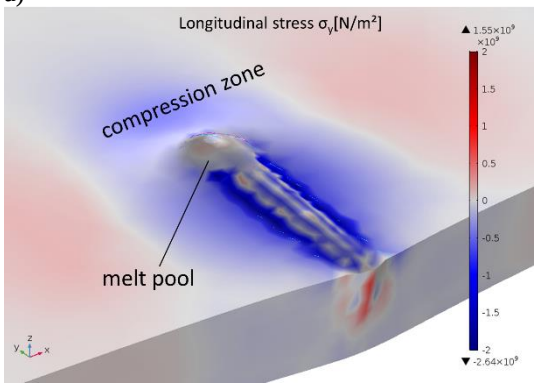

b)

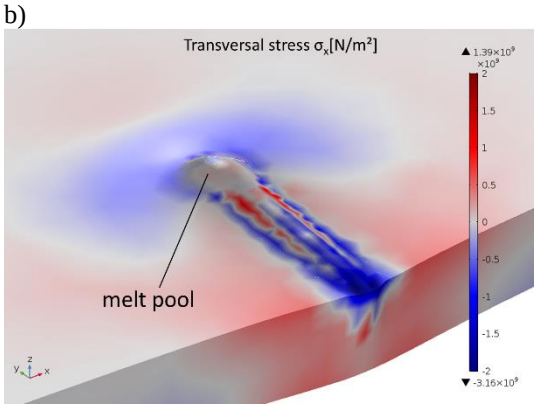

Figure 3. Stress distribution in the welding zone of a blind weld: a) longitudinal stress and b) transversal stress.

The extend of the molten track, where material has molten and/or solidified again, is tracked by a distributed ODE of the form:

$$\Phi_w = \begin{cases} \Phi_m & \text{for } \Phi_m > \Phi_w \\ \Phi_w & \text{for } \Phi_m \leq \Phi_w \end{cases}$$

Φ_w is the phase function of the molten track. In the simulation of laser beam welding in overlap configuration contact between the joining partners in the molten track (Φ_w=1) is modelled by a thin elastic layer in the region where the molten track connects the two sheets. In the remaining contact zone between the two sheets mechanical contact based on the penalty method is defined. Clamping of the sheets is modelled by spring foundations of high stiffness on the tool side and boundary loads on the respective clamping boundaries of the workpiece (Figure 4). The bottom sheet is fixed by three pointwise constraints. The top plate is held by the clamping force and after clamping removal it is fixed by the thin elastic layer in the molten track.

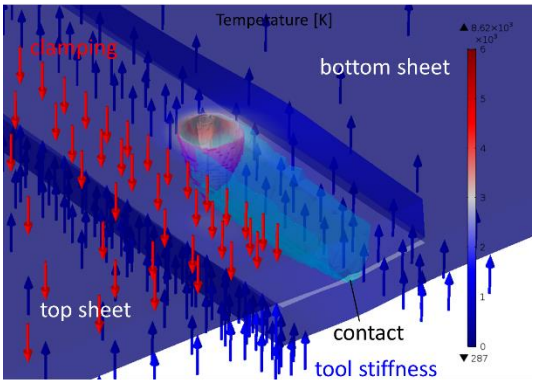

Figure 4. Simulation model for laser beam welding in overlap configuration.

For the calculation the sheet was meshed with swept triangular elements, with an element size in the order of the laser beam radius along the weld track. The applied mesh for the blind weld is shown in Figure 5.

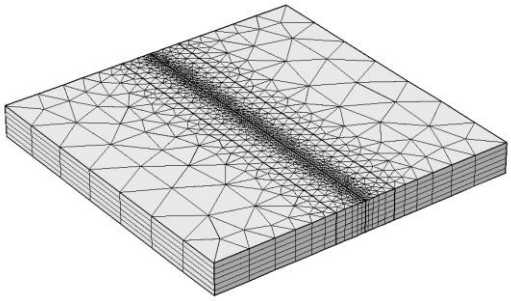

Figure 5. Computational mesh for laser beam welding simulation.

Simulation Results

The computational model was applied to simulate laser beam welding of molybdenum. The welding parameters and material data used for the simulations are listed in Tables 1 and 2, respectively.

Laser power	2000 W
Focus radius	100 µm
Feed rate	0.1 m/s
Clamping force	1e8 N/m²

Table 1: Welding parameters.

Absorption coefficient	0.8
Emissivity	0.2
Thermal conductivity	140 W/(m·K)
Density	10200 kg/m³
Specific heat capacity	250 J/(kg·K)
Thermal expansion coefficient	5e-6 1/K
Melting temperature	2873 K
Evaporation temperature	5833 K
Melting enthalpy	2.9e5 J/kg
Evaporation enthalpy	5.6e6 J/kg
Young's modulus	330e9 Pa
Poisson ratio	0.3
Initial yield stress	400e6 Pa
Isotropic tangent modulus	33e9 Pa

Table 2: Material data.

a)

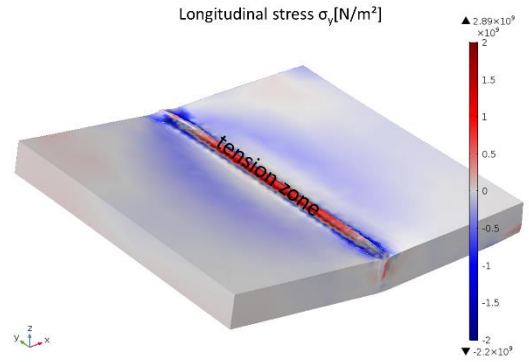

b)

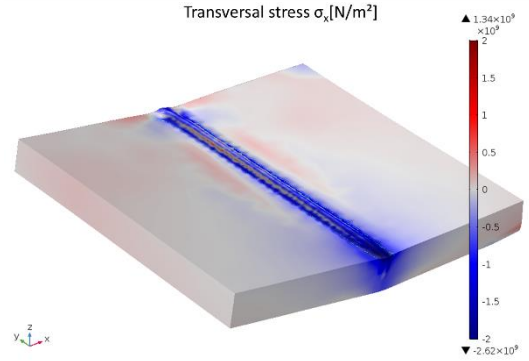

Figure 6. Stress distribution in a blind seam in laser beam welding: a) longitudinal residual stress and b) transversal residual stress.

For a first verification of the numerical model laser beam welding of a blind seam in a 1 mm unclamped molybdenum sheet was simulated. Figures 1 and 3 show the simulated temperature and stress distribution in the welding zone during the process. Figures 6 a and b show the finally obtained residual stress distribution in longitudinal and transversal direction in the processed sheet. The displacement is scaled by a factor of 10. In accordance to classical welding theory [13] the simulation model shows a compression region in front of the melt pool (Figure 3 a) and a tension zone in the weld seam (Figure 6 b). The final weld seam shows residual tensile stresses in longitudinal direction due to a shrinkage of the weld seam during cooling. In the supporting surrounding material residual compressive stresses are induced (Figure 6 a). In transversal direction residual stresses occur due to the shrinkage of the seam and as a reaction on the longitudinal residual stresses. In the middle of the seam residual tensile stresses occur due to a shortening of the seam, whereas at the beginning and ending residual compressive stresses dominate (Figure 6 b).

a)

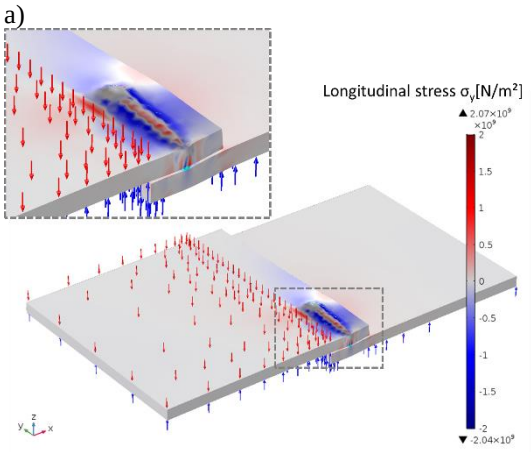

b)

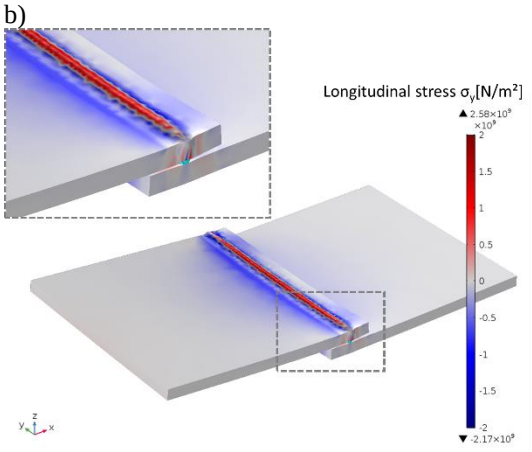

Figure 7. Longitudinal stress in laser beam welding in overlap configuration: a) during processing and b) after removal of the clamping.

a)

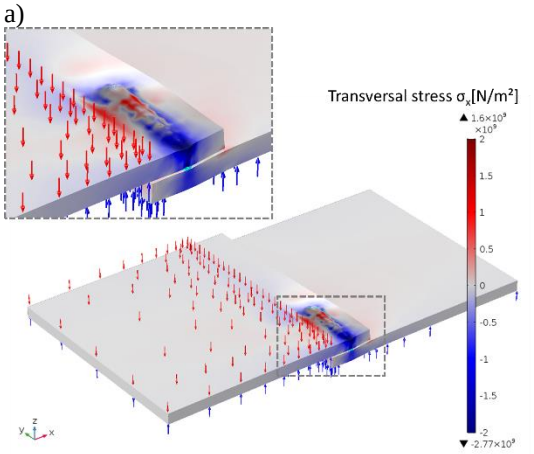

b)

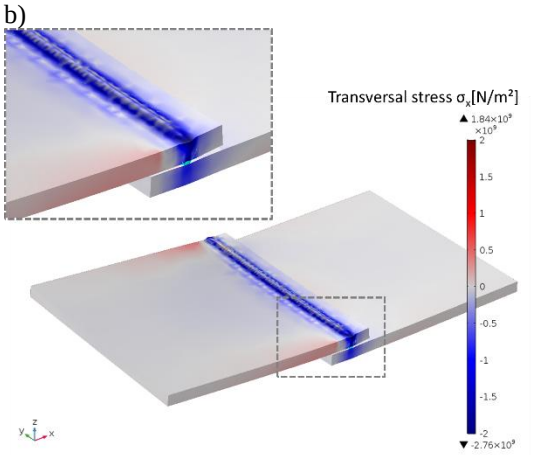

Figure 8. Transversal stress in laser beam welding in overlap configuration: a) during processing and b) after removal of the clamping.

Based on the simulation model, laser welding of two 0.5 mm molybdenum sheets in overlap configuration is analysed, too. Figure 4 shows the temperature field, the melt pool and the evolving weld seam during the process. Despite the camping lateral and vertical movement of the joining partners occurs due to thermal expansion in the joining zone (Figures 7 a and 8 a). After removal of the clamping force, the residual stresses in the weld lead to a folding of the joint sheets and finally a distortion of the workpiece (Figures 7 b and 8 b).

Based on those results the simulation model is applied to analyze the influence of welding strategy in laser beam welding of molybdenum sheets. At this laser beam joining of two 0.5 mm molybdenum sheets with a size of 70 mm x 40 mm by an array of 3 x 3 10 mm laser welds is regarded. At the bottom a rigid tool over the sheet area and from the top a clamping along the edge of the sheet with a width of 5 mm is assumed. For those simulations a coarser mesh with an element size of the laser beam diameter is applied to keep compute times sufficiently low.

a)

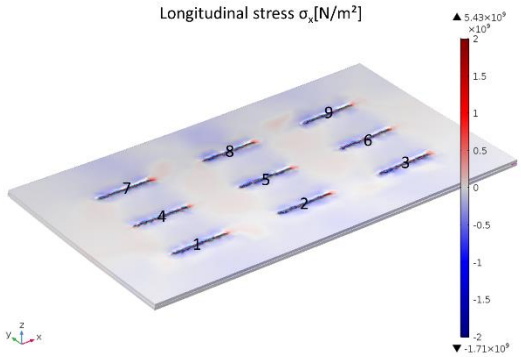

b)

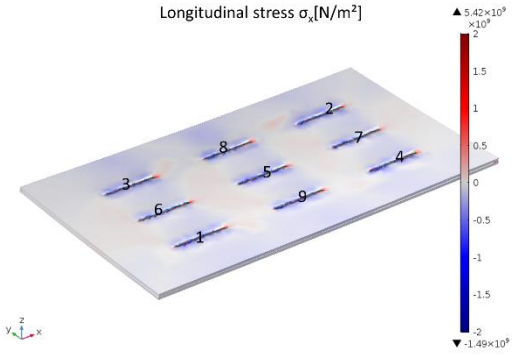

Figure 9. Longitudinal residual stress for different welding strategies: a) Welding strategy I; b) Welding strategy II.

a)

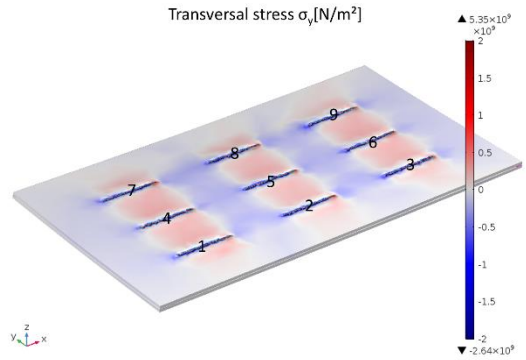

b)

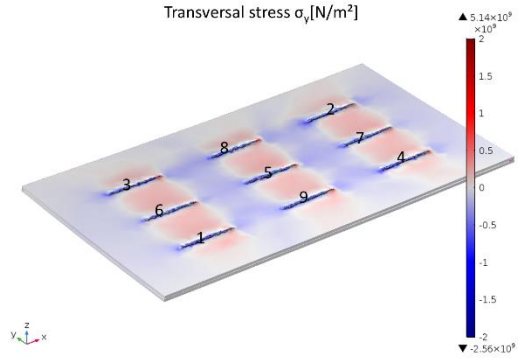

Figure 10. Transversal residual stress for different welding strategies: a) Welding strategy I; b) Welding strategy II.

Figures 9 and 10 show the residual stress distributions in longitudinal and transversal direction. Welding strategy I that does the welds in a sequence delivers higher transversal residual stresses compared to welding strategy II that tries to assure maximum distance between two following welds. This is an indication for a higher risk for crack formation. Also the final distortion for welding strategy I is slightly higher and the distortion pattern is less symmetric (Figure 11).

a)

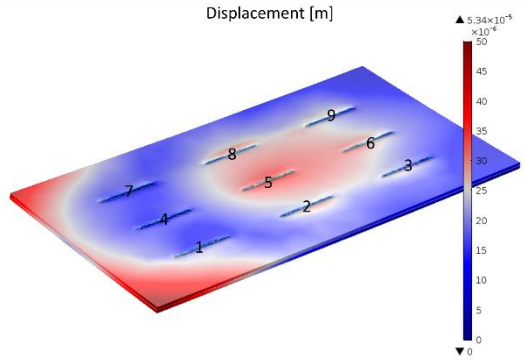

b)

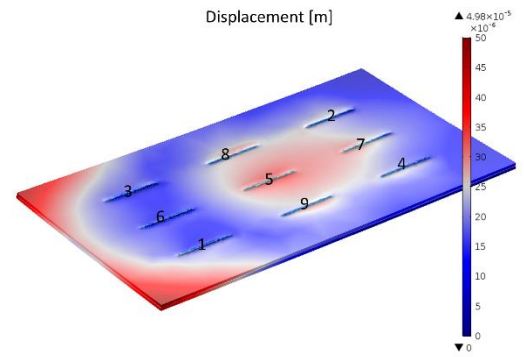

Figure 11. Distortion for different welding strategies: a) Welding strategy I; b) Welding strategy II.

Conclusions

The presented modelling approach for laser beam welding allows a description of the thermo-mechanical processes in laser beam welding. Both the stresses in the processing zone during the welding process and the stresses in the weld seam are obtained in accordance to welding theory. The modelling approach can be applied for a simulation of laser beam welding of molybdenum sheets in overlap configuration. Both clamping of the workpiece and the establishment of contact in the welding zone can be described. The presented approach can be applied to analyze the influence of different clamping configurations in laser beam welding. Furthermore, based on the presented simulation approach an analysis of different welding strategies for more complex workpieces as well as an optimization of welding strategies with respect to a minimization of residual stresses and distortion becomes feasible. The presented modelling approach is not restricted to laser

beam welding of molybdenum. It can be easily transferred to other welding technologies and processed materials.

References

[1] B. Tabernig, N. Reheis, Joining of Refractory Metals and its Application, Proceedings of the 17th Plansee Seminar, Vol. 4 (2009).

[2] W. Jiteng, W. Juan, L. Yajing, Z. Deshuang, Progress of Research on Welding of Molybdenum Alloys, High Temperature Material Proceedings, 33(3), 193-200 (2014).

[3] R. Lison, Schweißen von Molybdän und seinen Legierungen, Schweißen und Schneiden, 38, Heft 9, 437-441 (1986).

[4] B. V. Cockeram, E. K. Ohriner, T. S. Byun, M. K. Miller, L. L. Snead, Weldable ductile molybdenum alloy development, Journal of Nuclear Materials 382, 229-241 (2008).

[5] M. Geiger, K.-H. Leitz, H. Koch, A. Otto, A 3D transient model of keyhole and melt pool dynamics in laser beam welding applied to the joining of zinc coated sheets, Production Engineering, Volume 3, Issue 2, 127-136 (2009).

[6] A. Otto, H. Koch, K.-H. Leitz, M. Schmidt, Numerical Simulations – A Versatile Approach for Better Understanding Dynamics in Laser Material Processing, Physics Procedia 12, 11-20 (2011)

[7] M. Courtois, M. Carin, P. Le Masson, S. Gaided, M. Balabane, Guidelines in the experimental validation of a 3D heat and fluid flow model of keyhole laser welding, Journal of Physics D: Applied Physics, Vol. 49, No. 15 (2016).

[8] A. Otto, R. G. Vázquez, U. Hartel, S. Mosbah, Numerical analysis of process dynamics in laser welding of Al and Cu, Procedia CIRP 74, 691-695 (2018).

[9] P. Martinson, S. Daneshpour, M. Kocak, S. Riekehr, P. Staron, Residual stress analysis of laser spot welding of steel sheets, Materials & Design, Vol. 30, Issue 9, 3351-3359 (2009).

[10] F. Schlather, F. Theurer, F. Oefele, M. F. Zaeh, Process forces during remote laser beam welding and resistance spot welding – a comparative study, Procedia CIRP, Vol. 74, 669-673 (2018).

[11] M. Dal, R. Fabbro, An overview of the state of art in laser welding simulation, Optics & Laser Technology, Vol. 78, Part A, 2-14 (2016).

[12] H. Hügel, T. Graf, Fundamentals of laser-induced processes, Landolt-Börnstein, Vol. VIII/1C (2004).

[13] A. Otto, Transiente Prozesse beim Laserstrahlschweißen, Dissertation Universität Erlangen-Nürnberg, Meisenbach Verlag, Bamberg (1997).